

SOEDiff: Efficient Distillation for Small Object Editing

Qihe Pan
Zhejiang University of Technology
Hangzhou, Zhejiang, China
panqihe996@gmail.com

Yiming Wu
The University of Hong Kong
Hongkong, China
yimingwu0@gmail.com

Zicheng Wang
The University of Hong Kong
Hongkong, China
xiaoyao3302@outlook.com

Sifan Long
Jilin University
Changchun, Jilin, China
longsf22@mails.jlu.edu.cn

Zhen Zhao
University of Sydney
Sydney, Australia
zhen.zhao@sydney.edu.au

Haoran Liang
Zhejiang University of Technology
Hangzhou, Zhejiang, China
haoran@zjut.edu.cn

Ronghua Liang
Zhejiang University of Technology
Hangzhou, Zhejiang, China
rhliang@zjut.edu.cn

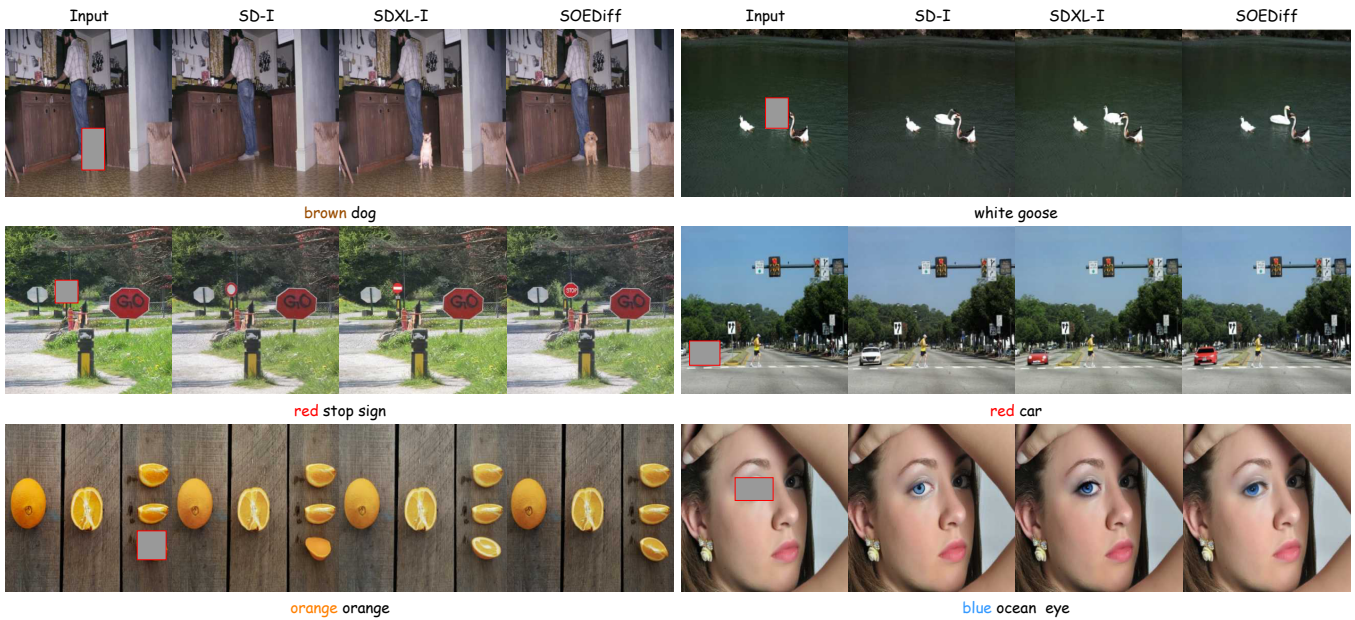


Figure 1: The image showcases examples of small object editing. The first column shows input images along with the masked small areas highlighted within red bounding boxes. The second column depicts results generated by SD-I [30]. In the third column, results produced by SD-XL [25] are presented. The fourth column features outcomes generated by our proposed SOEDiff model. Zoom in for a better view.

ABSTRACT

In this paper, we delve into a new task known as small object editing (SOE), which focuses on text-based image inpainting within a constrained, small-sized area. Despite the remarkable success have been achieved by current image inpainting approaches, their application to the SOE task generally results in failure cases such as *Object Missing*, *Text-Image Mismatch*, and *Distortion*. These failures stem from the limited use of small-sized objects in training datasets and the downsampling operations employed by U-Net models, which hinders accurate generation. To overcome these challenges, we introduce a novel training-based approach, SOEDiff,

Permission to make digital or hard copies of all or part of this work for personal or classroom use is granted without fee provided that copies are not made or distributed for profit or commercial advantage and that copies bear this notice and the full citation on the first page. Copyrights for components of this work owned by others than the author(s) must be honored. Abstracting with credit is permitted. To copy otherwise, or republish, to post on servers or to redistribute to lists, requires prior specific permission and/or a fee. Request permissions from permissions@acm.org.

ACM MM, 2024, Melbourne, Australia

© 2018 Copyright held by the owner/author(s). Publication rights licensed to ACM.

ACM ISBN 978-1-4503-XXXX-X/18/06

<https://doi.org/XXXXXXXX.XXXXXXX>

aimed at enhancing the capability of baseline models like StableDiffusion in editing small-sized objects while minimizing training costs. Specifically, our method involves two key components: **SO-LoRA**, which efficiently fine-tunes low-rank matrices, and **Cross-Scale Score Distillation loss**, which leverages high-resolution predictions from the pre-trained teacher diffusion model. Our method presents significant improvements on the test dataset collected from MSCOCO and OpenImage, validating the effectiveness of our proposed method in small object editing. In particular, when comparing SOEDiff with SD-I model on the *OpenImage-f* dataset, we observe a 0.99 improvement in CLIP-Score and a reduction of 2.87 in FID. Our project page can be found <https://soediff.github.io/>.

CCS CONCEPTS

• **Computing methodologies** → **Artificial intelligence**.

KEYWORDS

Small Object Editing, Image Editing, LoRA, Score Distillation

1 INTRODUCTION

The advent of diffusion models has marked a new era in the field of text-to-image generation, demonstrating the creation of intricate and coherent visual representations. Compared with generating entirely new images, image-editing models present particular excellence in manipulating regional aspects adjustment (*e.g.*, the appearance and objects) and holistic style transformation (*e.g.*, the structure, aesthetic, and style) of images. Despite the progress achieved by the recent researcher in generic-sized object editing, there has been a large oversight in addressing the requirement for subtle adjustments and fine-grained editing in extremely small areas (*e.g.*, changing the style of eyebrow or removing the barrettes). Given this perspective, we pose the question naturally: *What happens if we perform image editing in small areas?*

The constraints of editing in a confined small area pose significant challenges to conventional editing techniques, which we refer to as **Small Object Editing (SOE)**¹. As shown in Fig. 2, we present three typical types of failure cases: **Object Missing**, **Text-Image Mismatch**, and **Distortion**. These failures stem from two main factors. First, small-sized objects are rarely used in training image editing models, thereby restricting the capability to generate small objects. For instance, GLIGEN [17] discards the small-sized objects during the pre-processing of the training datasets. Consequently, lacking such training information can severely limit the ability to follow specific editing instructions on small objects and even lead to image distortion around the objects. Second, upon inspecting the architecture of the convolutional U-Net models, we find that the downsampling operation employed by StableDiffusion [30] impedes the accurate generation of small objects. Specifically, we denote the grids corresponding to the original bounding box in the feature maps as “effective area”, which diminishes in size due to multiple downsampling operations. For instance, within a 512×512 image, a 64×64 bounding box corresponds to an 8×8 grid in the first layer of UNet, and the effective area comes to 1×1 in lowest-resolution feature maps. This challenge intensifies the difficulty of accurately

¹In this paper, our focus is on the task of inpainting the object within a small-sized bounding box, which are subsequently used to create mask.

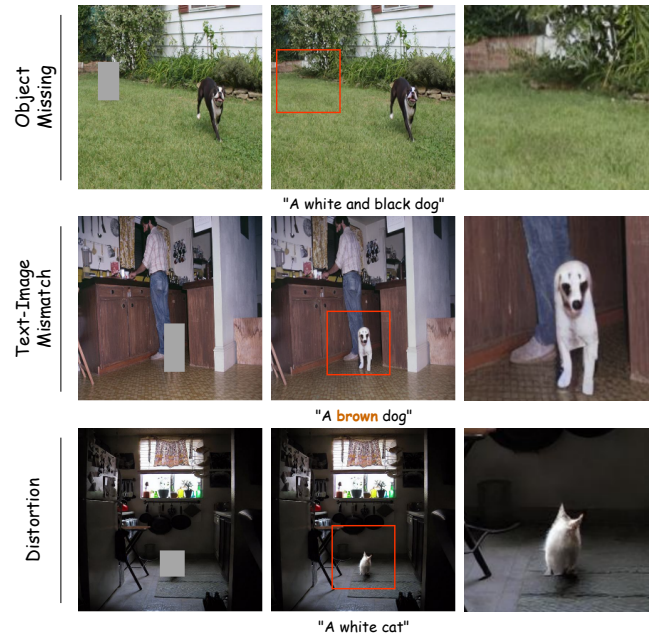


Figure 2: Challenges in inpainting small objects. Images are presented along with their corresponding masks, inpainted images, and enlarged inpainting areas in three separate columns. Three major challenges are presented: **Object Missing**, the model fails to generate the object as described in the text description; **T2I Mismatch**, the discrepancy between the generated content and the textual description, particularly in attributions like color or shape; **Distortion**, the generated object appears distorted, *e.g.*, the essential features like the cat’s face are missing in this image. Zoom in for a better view.

injecting the textual information into the corresponding “effective area” in the cross-attention layer².

To overcome the challenges, we propose a novel method termed SOEDiff, designed to improve the capabilities of base models (*e.g.*, StableDiffusion) in editing small-sized objects while minimizing training costs. To this end, two main components are involved in our approach: First, drawing inspiration from LoRA [13] that known for its efficiency in fine-tuning diffusion models, we propose the SO-LoRA, which aims to optimize low-rank matrices for small object editing, enhancing the alignment between textual descriptions and generated small objects. Second, we propose the Cross-Scale Score Distillation loss to further enhance the image quality. By leveraging insights from high-resolution predictions through a pre-trained teacher diffusion model, we mitigate blurriness and distortion typical in traditional diffusion models. Additionally, to further enhance the image fidelity, we fine-tune the VAE by performing pixel-level reconstruction. Our main contributions are as follows:

- We first time identify and address small object editing with a brand-new training-based approach termed SOEDiff. By

²We present a detailed analysis in Sec. 5.1

employing a lightweight fine-tuning module SO-LoRA, we verify that low-rank adaptation modules are sufficient to enhance the capabilities of pre-trained diffusion models in small object editing.

- We propose a Cross-Scale Score Distillation loss to effectively leverage the high-resolution representations from a teacher diffusion model, thereby enhancing the image fidelity.
- In contrast to previous text-based image editing approaches, our method presents prominent improvement on the test datasets collected from *MSCOCO* and *OpenImage* for small object editing. Specifically, by comparing SOEDiff with SD-I model on *OpenImage-f* dataset, we obtain a 0.99 improvement on CLIP-Score and reduce FID by 2.87.

2 RELATED WORK

2.1 Text-to-Image Diffusion

Diffusion models (DMs) [12, 23, 25, 29, 30] have emerged as the *de facto* standard in the domain of image generation, outperforming Generative Adversarial Networks (GANs) [10, 39, 41, 44, 46] in terms of both superior performance and training robustness. Denoising Diffusion Probabilistic Models (DDPM)[12] and Noise Conditional Score Networks (NCSN)[38] pioneered the utilization of denoising neural networks to invert a predefined Markovian noising process applied to raw images. Latent Diffusion Models (LDM)[30] intuitively disentangle image synthesis into two stages: semantic reconstruction through a denoising process in latent space, and perceptual reconstruction through decoding, such a strategy significantly enhances visual fidelity. Further advancing the design of effective network architectures, Imagen[32] integrates the capabilities of a pre-trained large language model (e.g., T5[27]) to enhance image-text alignment and introduces additional diffusion models for super-resolution, thereby generating images of larger sizes. Similarly, SDXL[25] extends the architecture by incorporating a larger denoising network and an extra refiner network, improving visual fidelity. DALLÉ-3 [4] enhances the prompt-following capabilities of DMs by training on highly descriptive captions generated through a bespoke image captioning process applied to the training dataset. Those diffusion models conditioned mainly on text prompts. ControlNet [45] and T2I-Adapter[22] indeed marks another significant milestone in the development of image-conditioned generation. Moving beyond the UNet-like architecture, DiTs[24] and U-Vit [3] have explored the replacement of UNet with transformer blocks, achieving superior performance by scaling up diffusion models.

Similar to the success in image synthesis domain, diffusion have had significant strides for editing images too. Imagic[14] is the first able to make complex non-rigid edits to real images by learning to align a text embedding with the input image and the target text. PnP[40], NTI[21], Imagic[14], DiffEdit[6] first use DDIM[36] inversion to invert the image to the input tensor, and then use the text conditioned denoising process to generate the image with the required edit. P2P[11] achieves modifications to synthesized images by utilizing attention control. InstructPix2Pix [5] and Imagen Editor[32] pass the image to be edited directly to the diffusion model by bypassing the DDIM inversion step. DiffusionCLIP [15] leveraged the capability of CLIP [26] to perform image-text feature

alignment to achieve the text-driven editing of the image. Blended-Diffusion [1, 2] explore the method of using a mask to edit the specific region and add a new object to the image while leaving the rest unchanged, while ESD[8] and Inst-Inpaint [42] focus on erasing the concept in the image by instructions.

2.2 Parameter-efficient Fine-tuning (PEFT)

Parameter-efficient fine-tuning (PEFT) concentrates on fine-tuning and optimizing model parameters in a way that conserves resources. This strategy is designed to boost a pre-trained model's efficacy for particular tasks or areas, avoiding the need for substantial extra data or computational power. Through the targeted adjustment of a select group of parameters, PEFT effectively adapts the model, proving to be highly beneficial in situations where labeled data is scarce or computational resources are restricted. Among many PEFT methods, the method based on reparameterization is the most representative and has been widely researched. LoRA [13] leverages low-rank approximations to efficiently fine-tune the model parameters, enabling more effective adaptation while mitigating computational demands. Specifically tailored for Stable Diffusion models, LoRA offers a promising avenue to enhance adaptability and performance in generative tasks involving diffusion processes. ControlNet[45] and T2I-Adapter[22] employs LoRA to process a variety of image prompts, enabling broad control over image characteristics. It allows various conditional inputs, such as edge, pose, to control the image generation process. Latent consistency model (LCM) [18] leverages LoRA and distillation tech for model acceleration during the sampling process and achieved great success. ConceptSliders [9] and ContinualDiffusion [35] using LoRA to achieve more precise control. At the same time, LoRA can also be used with Dreambooth[31] to help the model learn a new concept, which can be an object or a style.

2.3 Diffusion Distillation

Distillation technology is widely utilized for accelerating the sampling tasks in diffusion models. In the diffusion distillation framework, a student model is trained to distill the multi-step outputs of the original diffusion model into fewer steps. Progressive Distillation [33] train a series of student model by repeated distillation. Adversarial Diffusion Distillation(ADD)[34], uses a pretrained feature extractors as its discriminator, achieving great performance in only four steps. Consistency Model(CM)[37] employ a consistency mapping tech to achieve one-step generation. Inspired by CM, LCM [18] solve the reverse diffusion process by treating it as a probability flow ODE (PF-ODE) problem in the latent space. And LCM-LoRA[19] introduce a LoRA training for efficiently learning LCM modules. SD3-Turbo apply ADD to SD3(8B) [7] to achieve the goal of fast high-resolution image synthesis.

In our paper, we are motivated by existing work in the field, and we have designed a LoRA specifically aimed at addressing the issue of small object generation with distillation. Our method fills a critical gap in the current landscape, offering a more universal and accurate solution for this challenge. This advancement not only improves upon the existing methodologies but also broadens the scope of applicability in the domain of diffusion models for image generation.

3 PRELIMINARIES

3.1 Diffusion Models

Diffusion model is a kind of generative model that reverses the diffusion process to synthesize data. Initially, the forward diffusion process gradually adds noise to the data, transitioning it from a data point x_0 to the complete Gaussian noise x_T . At any timestep t , the noised image is modelled as:

$$x_t = \sqrt{1 - \beta_t} x_0 + \sqrt{\beta_t} \epsilon, \quad (1)$$

where ϵ is randomly sampled Gaussian noise with zero mean and unit variance, and β_t is controlled by a variance scheduler $\{\beta_t \in (0, 1)\}_{t=1}^T$. Diffusion models aim to reverse this diffusion process by sampling random Gaussian noise x_T and gradually denoising the image to generate an image x_0 . In practice, denoising network ϵ_θ learns to reverse the diffusion process by predicting the sampled noise ϵ , optimizing the following Mean Square Error:

$$\mathcal{L} = \mathbb{E}_{x_t, c, t, \epsilon \sim \mathcal{N}(0,1)} \|\epsilon - \epsilon_\theta(x_t, c, t)\|_2^2, \quad (2)$$

where x_t , t , and c are the noised image, timestep, and condition, respectively. In this paper, we study with StableDiffusion (SD), a latent diffusion model designed to enhance sampling efficiency while preserving image quality. This method employs an iterative denoising process within a low-dimensional latent space, facilitated by a pre-trained variational autoencoder (VAE). SD runs the reverse process in the latent space to obtain denoised latent feature \hat{z}_0 , and then decodes \hat{z}_0 through the VAE decoder to get the predicted image \hat{x}_0 .

3.2 Low-Rank Adaptation

The Low-Rank Adaptation (LoRA) method facilitates the efficient adaptation of large pre-trained models to downstream tasks by decomposing the weight update ΔW during fine-tuning. Given a pre-trained model layer with weights $W_0 \in \mathbb{R}^{j \times k}$, where j is the input dimension and k is the output dimension, ΔW is decomposed into two low-rank matrices $\Delta W = BA$, where $B \in \mathbb{R}^{j \times r}$, $A \in \mathbb{R}^{r \times k}$ and $r \ll \min(j, k)$. During initialization, the entries of B are all set to zero to ensure $\Delta W = 0$ at the beginning of training, and A is initialized with Gaussian distribution. By freezing W_0 and optimizing only the matrices A and B , LoRA achieves significant reductions in trainable parameters. During inference, ΔW can be merged into W_0 with no additional computation/memory overhead using a scaling factor α :

$$W = W_0 + \alpha \Delta W = W_0 + \alpha BA \quad (3)$$

4 METHODOLOGY

Our method introduces an innovative approach, SOEDiff, to significantly enhance the generation of small object in image synthesis. We strategically design a specialized SO-LoRA module (Sec. 4.2) to improve the alignment of image and text within the small area. Complementing this, our approach integrates a cross-scale score distillation loss (Sec. 4.3), aimed at enhancing the quality of generated small objects by distilling knowledge from models trained on generic-sized objects. By combining these two techniques, our method achieves a significant improvement in the SOE task.

4.1 Overview

Let $\{x_i, m_i, c_i\}_{i=1}^N$ denotes the samples from the training dataset, where N is the number of data samples, x_i represents the image, m_i corresponds to the mask (bounding box), and c_i is the textual description. As depicted in Fig. 3, our training pipeline involves multiple networks: a teacher model ϵ_ϕ , a student model ϵ_θ , and the encoder \mathcal{E} and decoder \mathcal{D} of an autoencoder. We elaborate on each module in our method as follows:

Image Autoencoder: In line with typical latent diffusion models [25, 30], the image x (omitting subscript i for clarity) undergoes projection into the latent space with a pre-trained image encoder \mathcal{E} to obtain the latent feature z , which could be reconstructed into an image using the image decoder \mathcal{D} .

Text Encoder: Textual description generally serve to control the generated content, leveraging models like CLIP [26] and T5 [28], pre-trained on large-scale text-image pairs, for text feature extraction. In our SOEDiff approach, we adopt text encoder from CLIP to encode textual description c into a text feature $\mathcal{E}^{text}(c)$.

SO-LoRA: Our method incorporates two diffusion models initialized with pre-trained SD/SDXL. During the training stage, the teacher diffusion model ϵ_ϕ remains frozen, while we integrate the adapter SO-LoRA with the student diffusion model ϵ_θ , in which only parameters of SO-LoRA are updated for fast adaptation.

Optimization: We introduce three objective losses, denoted as $\mathcal{L}_{denoise}$, $\mathcal{L}_{distill}$, and \mathcal{L}_{vae} , to optimize the image autoencoder and the SO-LoRA module. For $\mathcal{L}_{denoise}$, we apply the diffusion process on the latent feature z as described in Eq. 1 to obtain the noised latent z_t , which is then fed into the student model to predict the noise ϵ with $\epsilon_\theta(z_t, c, t, m)$. For $\mathcal{L}_{distill}$, we begin by center-cropping the image around the target object to obtain the re-scaled image x' and mask m' , which are then input into the teacher diffusion model to acquire the re-scaled predicted noise $\epsilon_\phi(z'_t, c, t, m')$, where z'_t is latent feature extracted by the image encoder. We enforce the prediction from student model to be close to prediction from teacher's by minimizing $\mathcal{L}_{distill}$. Finally, since the VAE model is critical for generating high-fidelity small object, we further fine-tune the encoder and decoder to enhance detail preserving with a reconstruction loss $\mathcal{L}_{vae}(x, \mathcal{D}(\mathcal{E}(x)))$, where we use the Huber loss for robust regression. Thus, we optimize the network with a total loss:

$$\begin{aligned} \mathcal{L}_{total} = & \mathcal{L}_{denoise}(\epsilon, \epsilon_\theta(z_t, c, t, m)) \\ & + \alpha \mathcal{L}_{distill}(\epsilon_\theta(z_t, c, t, m), \epsilon_\phi(z'_t, c, t, m')) \\ & + \lambda \mathcal{L}_{vae}(x, \mathcal{D}(\mathcal{E}(x))). \end{aligned} \quad (4)$$

We will subsequently elaborate on these objective losses in the following sections.

4.2 SO-LoRA

In designing our SO-LoRA module, we have adhered to the principle established in LCM [18] and ControlNet [45] designs. The structure of our SO-LoRA is the same the backbone network. During the training phase, only the SO-LoRA module in the student model ϵ_θ is trainable.

Given an input image x and the corresponding mask m , we encode the image x with the encoder \mathcal{E} to get latent feature z and progressively adding noise to z to yield a noisy latent z_t , where t

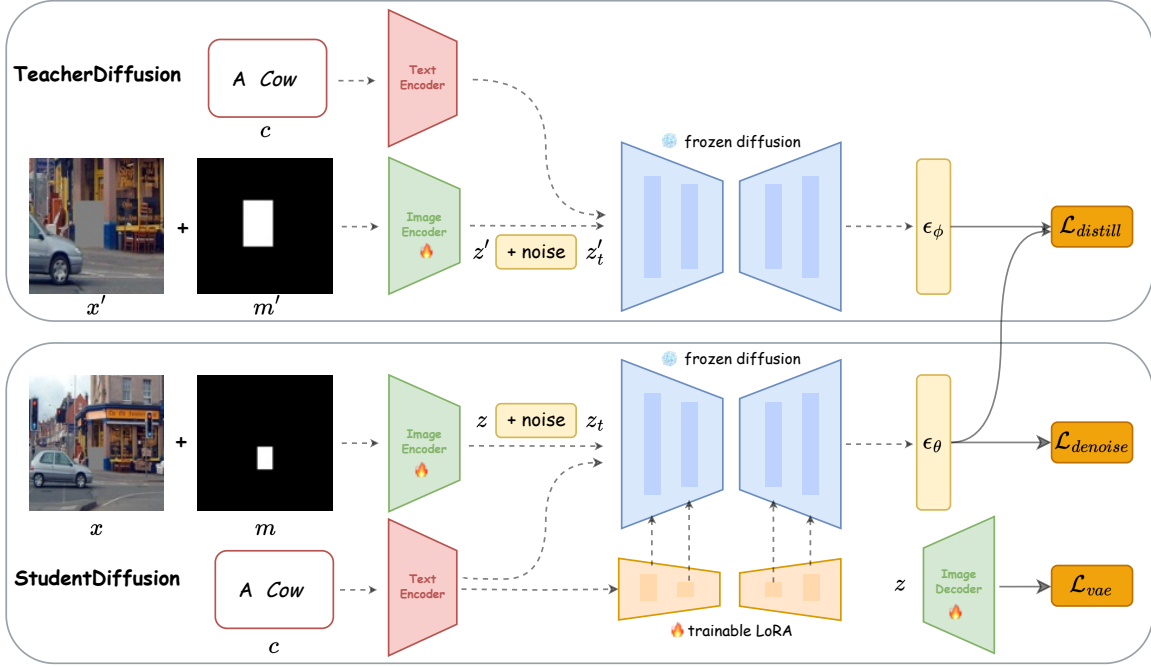


Figure 3: Overview of our proposed SOEDiff. The student diffusion receives smaller-mask image x , mask m , text prompt c as input and the teacher diffusion receives cropped larger-sized mask image x' , mask m' , as input to optimize three objectives: a) denoising loss: the student model aims to predict the noise ϵ_θ to match the noise added ϵ in the diffusion forward process. b) distillation loss: the student model is trained to generate the same content within the mask region as generated by the teacher model. c) reconstruction loss: the VAE model is trained to reduce information loss in small target regions.

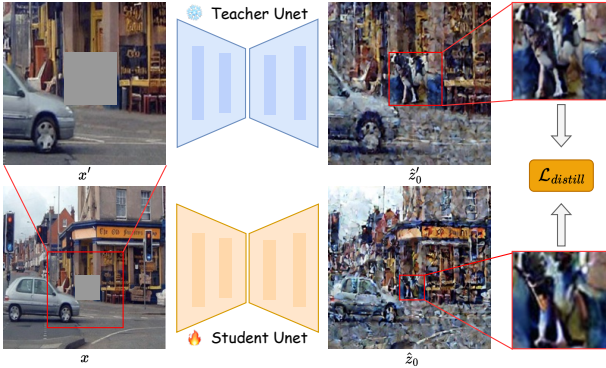


Figure 4: The teacher model receives cropped and resized image as inputs, while the student model processes smaller one. These models predict noises \hat{z}_0 and \hat{z}'_0 respectively following Eq. 6, and then resize their respective predicted noises to calculate the distillation loss $\mathcal{L}_{distill}$. (We omit the image feature encoding and noise addition processes for simplicity).

represents the timestep. To refine SO-LoRA for the task of generating small objects, denoising loss is calculated within the masked area. This focus ensures that SO-LoRA’s training and subsequent operations are concentrated on the small target regions, so that it

can precisely enhance alignment between the target region and the corresponding textual description. The denoising loss is formulated as follows:

$$\mathcal{L}_{denoise} = \mathbb{E}_{z_t, t, c, m, \epsilon \sim \mathcal{N}(0,1)} \mathcal{L}(\epsilon \odot m, \epsilon_\theta(z_t, t, c, m) \odot m), \quad (5)$$

where \mathcal{L} is the Huber loss.

4.3 Cross-Scale Score Distillation

To enhance the quality of generated small object images, we introduce an additional teacher model with weight ϕ for cross-scale distillation, leveraging high-resolution predictions as guidance. As previously mentioned, the student model takes the noised image feature z_t , mask m , and corresponding text prompt c as inputs, then predicts noise $\epsilon_\theta(z_t, t, c, m)$. For the teacher model, we first crop a region with a size of s centered around the masked area of the original image x and resize it to a new image x' with the same size as x . Then, we feed x' into the image encoder \mathcal{E} to obtain z' . Similar to the student model, we obtain the predicted noise $\epsilon_\phi(z'_t, t, c, m')$. In this enlarged masked area, we assume that more details are preserved and the prediction of the teacher model is more reliable. Therefore, we consider the reverse diffusion process as an augmented Probability Flow Ordinary Differential Equation (PF-ODE) following LCM [19], and then revert the predicted noise $\epsilon_\theta(z_t, t, c, m)$ (resp. $\epsilon_\phi(z'_t, t, c, m')$) to image \hat{z}_0 (resp. \hat{z}'_0) as follows:

$$\hat{z}_0 = \frac{z_t - \sigma_t \epsilon_\theta(z_t, t, c, m)}{\alpha_t}, \quad (6)$$

Algorithm 1: Algorithm of SOEDiff

```

1 Input: teacher model parameter  $\phi$ , student model
  parameter  $\theta$ , autoencoder  $\mathcal{E}(\cdot)$ ,  $\mathcal{D}(\cdot)$ , learning rate  $\eta$ ,
  noise schedule  $\alpha_t, \sigma_t$ , timestep  $t$ , distance loss  $\mathcal{L}(\cdot, \cdot)$ 
2 repeat
3   Sample image  $x$ , mask  $m$ , prompt  $c$  from Dataset
4   Crop and resize  $x$  to obtain  $x'$ 
5   Crop and resize  $m$  to obtain  $m'$ 
6   Encode images to latent space  $z \leftarrow \mathcal{E}(x)$ ,  $z' \leftarrow \mathcal{E}(x')$ 
7   Calculate the reconstruction loss
    $\mathcal{L}_{vae} = \mathcal{L}(x \odot m, \mathcal{D}(\mathcal{E}(x)) \odot m)$ 
8   Add noise to the latent features  $z_t \sim \mathcal{N}(\alpha_t z; \sigma_t^2 \mathbf{I})$ ,
    $z'_t \sim \mathcal{N}(\alpha_t z'; \sigma_t^2 \mathbf{I})$ 
9   Calculate the denoising loss  $\mathcal{L}_{denoise}$  as presented in
   Eq. 5
10  Revert noise to the image  $\hat{z}_0 \leftarrow f_\theta(z_t, t, c, m)$ ,
    $\hat{z}'_0 \leftarrow f_\theta(z'_t, t, c, m')$ 
11  Calculate the distillation loss  $\mathcal{L}_{distill}$  as presented in
   Eq. 7
12   $\theta \leftarrow \theta - \eta \nabla_\theta (\mathcal{L}_{denoise} + \mathcal{L}_{distill} + \mathcal{L}_{vae})$ 
13 until convergence

```

where σ_t and α_t are calculated from the predefined variance scheduler β . Next, features corresponding to the masked area are cropped from predictions \hat{z}_0 and \hat{z}'_0 . Then we resize these two features and align them with the following distillation loss:

$$\mathcal{L}_{distill} = \mathcal{L}(r(\hat{z}_0 \odot m), r(\hat{z}'_0 \odot m')), \quad (7)$$

where $r(\cdot)$ denotes the operation to resize the cropped latent feature to the same size, and \mathcal{L} is the Huber loss. We summarize the algorithm of SOEDiff in Alg. 1.

5 EXPERIMENTS

5.1 Analysis of Challenges in Generating Small Objects with StableDiffusion

We delve into the challenges encountered when generating small objects with StableDiffusion (SD). As illustrated in Fig. 5, the size of the cross attention map progressively diminishes as the depth increases. At the mid-block (depicted in the top parallelogram), the size of the cross attention map is 8×8 , with each side length being $1/8$ of the original latent code z . At this juncture, the corresponding feature map size dwindles to 1×1 . The diminutive size of this masked area poses a challenge as it may lack sufficient semantic information essential for generating associated objects.

5.2 Datasets

Training Data. To build our training dataset, we curated data from the vast *OpenImage* dataset, imposing rigorous standards to guarantee the data’s suitability for our small object editing task. We selected objects meeting specific criteria: they had to be unobscured, fully contained within the image boundaries, and represent tangible real-world entities. Furthermore, these objects had to exist individually rather than as part of a larger group, and they must

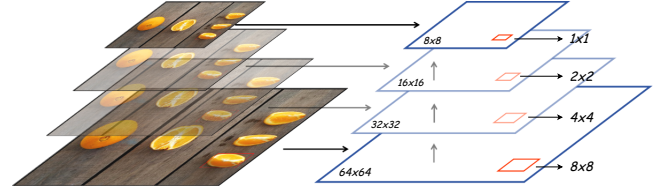


Figure 5: The illustration of cross-attention map. For a input image with size of 512×512 , if the masked area is 64×64 , the corresponding effective area comes to 1×1 in the mid-block. The diminutive size of this masked area poses a challenge as it may lack sufficient semantic information essential for generating associated objects.

not include human body parts like eyes or mouths. Crucially, the area occupied by these objects had to be less than $(1/8)^2$ of the total image area.

Validation Data. For our validation data, we carefully curated subsets from the *MSCOCO-val* and *OpenImage-val* datasets, specifically focusing on data where object sizes range between $(1/8)^2$ and $(1/6)^2$ of the image area. This selection process adheres to the same criteria used for curating the training dataset. The selected test data ensures that objects are unobstructed by other elements, resulting in two customized test datasets: *MSCOCO-f* and *OpenImage-f*. Moreover, we cropped the images to extract regions within the masked areas and employed the BLIP-VQA [16] model to inquire about the primary color of the object in each area. This method efficiently identifies the predominant colors of objects within the masks. The *OpenImage-f* dataset encompasses over 250 common categories, totaling approximately 2,000 images. In comparison, the *MSCOCO-f* dataset comprises images from 80 distinct categories, also amounting to about 2,000 images. Furthermore, we incorporated the complete *MSCOCO-val* and *OpenImage-val* datasets as additional validation datasets.

Size Threshold Analysis. Upon analysis, we identified the thresholds of $1/6$ and $1/8$ as critical for training and evaluation on small object editing. Our objective is to accurately generate small objects within this threshold. When the mask’s side length occupies $1/5$ of the image size, the corresponding 8×8 cross-attention map should ideally have feature side lengths of at least $\text{round}(8/5) = 2$. Similarly, if the mask’s side length is $1/6$ of the original image, the corresponding feature size decreases to 1×1 . In scenarios where the side length is smaller than $1/8$, it is even plausible that no corresponding features exist. The model’s training data comprises challenging examples aimed at enhancing its learning and performance. Furthermore, this approach ensures a more equitable validation process, given that the model has not been exposed to objects sized between $1/8$ and $1/6$ during the training phase.

Evaluation Metrics. We utilize the Fréchet Inception Distance (FID) to measure image quality and CLIP-Score to assess text-to-image alignment, following the evaluation protocol used in DDPM [12]. Higher CLIP-Score or lower FID values indicate superior performance. Importantly, we compute these metrics specifically on the masked areas, rather than employing the entire image for evaluation. This evaluation protocol is motivated by the fact that



Figure 6: Qualitative comparison of different components.

Table 1: Quantitative results on *OpenImage-f* and *MSCOCO-f*. SOEDiff significantly surpasses the baselines.

Prompt	Methods	OpenImage-f		MSCOCO-f	
		CLIP-Score	FID	CLIP-Score	FID
label	Blended DM	23.66	43.20	22.83	38.78
	SD-I	23.79	34.65	22.55	30.78
	SOEDiff	24.78	31.78	23.89	29.40
	SDXL-I	25.56	34.26	24.50	31.26
	SOEDiff-XL	26.17	31.33	25.32	29.25
color + label	Blended DM	23.85	43.26	22.94	38.01
	SD-I	24.13	34.73	22.66	30.65
	SOEDiff	25.57	31.21	24.38	27.62
	SDXL-I	25.81	34.87	24.46	31.23
	SOEDiff-XL	26.83	31.11	25.52	29.07

small objects occupy a relatively minor proportion of the overall image. Calculating metrics using the entire image could disproportionately bias the evaluation towards large, irrelevant areas, thus distorting the assessment of the model’s performance.

5.3 Text-based Small Object Editing

Implementation Details: For our experiments, we employed Stable-Diffusion-v1-5-Inpainting (SD-I) and Stable-Diffusion-xl-1.0-inpainting (SDXL-I) as the base models, along with the DDIM-Solver for fast inference. We maintained a batch size of 8 and conducted training for 100K steps. It’s worth noting that fine-tuning the VAE concurrently significantly increases computation cost, necessitating a reduction in batch size and prolonging the training duration. Regarding loss weights, we set α to 0.01 and λ to 1 to ensure that

Table 2: Quantitative results on full-sized datasets *OpenImage-val* and *MSCOCO-val*.

Prompt	Methods	OpenImage-val		MSCOCO-val	
		CLIP-Score	FID	CLIP-Score	FID
label	SD-I	25.08	7.81	23.09	6.88
	SOEDiff	25.52	6.80	23.68	6.30
color + label	SD-I	26.21	7.72	23.23	6.65
	SOEDiff	26.89	6.69	24.07	6.22

the initial losses of all components are aligned at the same order of magnitude. Additionally, the crop size s was set to 256 in our experiments.

Quantitative Result: We compared models trained on both backbones, SD-I and SDXL-I, alongside the mask-conditioned object generation model, BlendedDM [2] (based on SD-1.5). Additionally, we evaluated them on our filtered datasets, *OpenImage-f* and *MSCOCO-f*, using two types of prompt templates: label (e.g., “a dog”) and color+label (e.g., “a brown dog”). The results are shown in Tab. 1. Our method demonstrated a significant improvement compared to the baseline models on these two datasets, affirming the efficacy and superiority of our approach for small object generation. Some questions may arise regarding instances where the FID scores of the SDXL model appear lower in certain comparative scenarios such as *MSCOCO-f* dataset. This phenomenon has also been observed in SDXL [25]. It’s essential to note that higher FID scores do not necessarily correlate with worse visual outcomes. Furthermore, the SDXL’s generation of 512×512 images, which can lead to poorer outcomes, may also contribute to these discrepancies. In addition

Table 3: Effectiveness of the components adopted in SOEDiff. We employ SD-I as the base model for comparison.

Component	OpenImage-f				MSCOCO-f			
	SD-I	SO-LoRA	CSD	VT	CLIP-Score	FID	CLIP-Score	FID
✓					24.10	34.73	22.66	30.65
✓	✓				24.93	33.78	23.53	29.60
✓	✓		✓		25.16	33.98	23.67	29.24
✓	✓	✓			25.40	32.41	24.14	28.40
✓	✓	✓	✓		25.58	31.21	24.38	27.62

Table 4: CLIP-Score computed with different loss weight λ on *OpenImage-f* and *MSCOCO-f*.

dataset	λ			
	0.1	0.01	0.005	0.001
OpenImage-f	25.08	25.40	25.32	25.21
MSCOCO-f	23.83	24.38	24.28	24.16

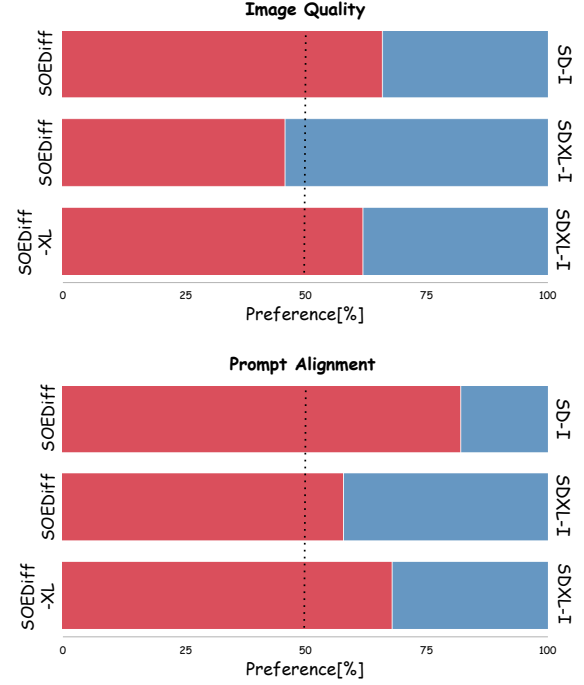
Table 5: CLIP-Score computed with different crop size s on *OpenImage-f*.

dataset	s			
	128	128~256	256	256~512
OpenImage-f	25.25	25.33	25.40	25.36
MSCOCO-f	24.12	24.30	24.38	24.28

to testing on the filtered dataset, we conducted evaluations on the full-sized *OpenImage-val* and *MSCOCO-val* datasets. This allowed us to demonstrate that our method is not only effective for small target objects but also beneficial for enhancing generic-sized object inpainting task. The results are presented in Tab. 2. All experiments were conducted at a standardized resolution of 512×512 pixels.

Effectiveness of Modules: As reported in Tab. 3, we validate the effectiveness of each module by testing different combinations of them with color+label as text prompt. Our observations reveal that both SO-LoRA and Cross-Scale Distillation (CSD) play significant roles in improving performance. Additionally, VAE Tuning (VT) contributes to enhancing the generation of detailed images. To provide more concrete evidence, we present visual comparisons in Fig. 6, and we find that the incorporation of SO-LoRA notably improves text-to-image alignment and mitigates the issues as illustrated in Fig. 2. Furthermore, the inclusion of both CSD and VT further refines the generated objects, resulting in overall higher-quality results.

Analysis of Loss Weight λ and Crop Scale s : In this section, we discuss two primary hyperparameters: the loss weight λ and the crop size s , used when inputting the cropped original small object images into the teacher model. In this experiment, we use the mainly proposed SO-LoRA and Cross-Scaled Distillation components to test the effect of λ and s on *OpenImage-f* and color+label as prompt. The main experimental results are presented in the Tab. 4 and Tab. 5. We found that varying the crop size s limited impact on the overall experimental results and conclusions. However, the setting of the λ is crucial to the experiment. When this loss weight is set too high, it leads to a significant decrease in performance and may even prevent the model from optimizing effectively.

**Figure 7: User preference study. We compare the performance of SOEDiff against baselines SD-I and SDXL-I.**

User Preference Study. Besides the automated metrics, we also incorporated a user study to align more closely with intuitive human preference. In the study, we aim to assess both prompt adherence and the overall image quality. We employed SD-I, SOEDiff, SDXL-I, and SOEDiff-XL as comparison models, keeping the seed fixed to generate 25 sets, totaling 100 images. Our study involved 100 total participants. Participants were tasked with ranking images of small target objects generated by the four models. Fig. 7 presents the user study. The most important results are: SOEDiff significantly enhances the base model's ability to improve both the image quality of generated objects and their alignment with the associated text.

Extended Applications: Apart from its core functionalities, our model also demonstrates proficiency in object removal and replacement, yielding favorable outcomes. This feature is particularly beneficial in the realm of image editing. As demonstrated in the image, it is possible to specify a target area and, guided by textual input, achieve the erasure or replacement of the designated object. Some examples are presented in Fig. 8.

6 CONCLUSION

In this study, we present our novel approach SOEDiff to enhancing small object editing with diffusion models. Our method begins with the integration of SO-LoRA tailored specifically for the SOE task. By incorporating a cross-scale score distillation loss, the high-resolution representations from a teacher diffusion model is leveraged for more precise generation of small objects guided by textual descriptions. This accomplishment represents a significant advancement in addressing this particular challenge.

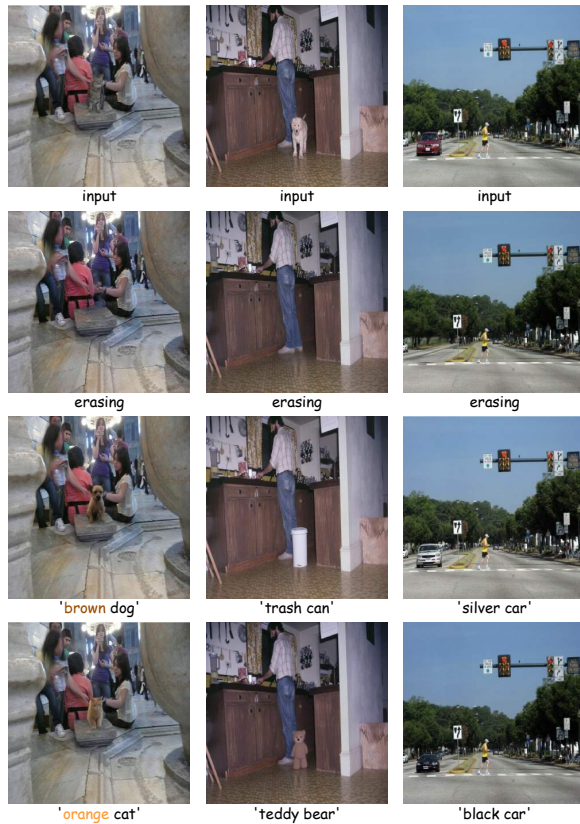


Figure 8: Extended application with our proposed SOEDiff.

REFERENCES

[1] Omri Avrahami, Ohad Fried, and Dani Lischinski. 2023. Blended latent diffusion. *ACM Transactions on Graphics (TOG)* 42, 4 (2023), 1–11.

[2] Omri Avrahami, Dani Lischinski, and Ohad Fried. 2022. Blended diffusion for text-driven editing of natural images. In *Proceedings of the IEEE/CVF Conference on Computer Vision and Pattern Recognition*. 18208–18218.

[3] Fan Bao, Shen Nie, Kaiwen Xue, Yue Cao, Chongxuan Li, Hang Su, and Jun Zhu. 2023. All are worth words: A vit backbone for diffusion models. In *Proceedings of the IEEE/CVF Conference on Computer Vision and Pattern Recognition*. 22669–22679.

[4] James Betker, Gabriel Goh, Li Jing, Tim Brooks, Jianfeng Wang, Linjie Li, Long Ouyang, Juntang Zhuang, Joyce Lee, Yufei Guo, et al. 2023. Improving image generation with better captions. *Computer Science*. <https://cdn.openai.com/papers/dall-e-3.pdf> 2, 3 (2023), 8.

[5] Tim Brooks, Aleksander Holynski, and Alexei A Efros. 2023. Instructpix2pix: Learning to follow image editing instructions. In *Proceedings of the IEEE/CVF Conference on Computer Vision and Pattern Recognition*. 18392–18402.

[6] Guillaume Couairon, Jakob Verbeek, Holger Schwenk, and Matthieu Cord. 2022. Diffedit: Diffusion-based semantic image editing with mask guidance. *arXiv preprint arXiv:2210.11427* (2022).

[7] Patrick Esser, Sumith Kulal, Andreas Blattmann, Rahim Entezari, Jonas Müller, Harry Saini, Yam Levi, Dominik Lorenz, Axel Sauer, Frederic Boesel, et al. 2024. Scaling rectified flow transformers for high-resolution image synthesis. *arXiv preprint arXiv:2403.03206* (2024).

[8] Rohit Gandikota, Joanna Materzynska, Jaden Fiotto-Kaufman, and David Bau. 2023. Erasing concepts from diffusion models. In *Proceedings of the IEEE/CVF International Conference on Computer Vision*. 2426–2436.

[9] Rohit Gandikota, Joanna Materzynska, Tingrui Zhou, Antonio Torralba, and David Bau. 2023. Concept sliders: Lora adaptors for precise control in diffusion models. *arXiv preprint arXiv:2311.12092* (2023).

[10] Ian Goodfellow, Jean Pouget-Abadie, Mehdi Mirza, Bing Xu, David Warde-Farley, Sherjil Ozair, Aaron Courville, and Yoshua Bengio. 2014. Generative adversarial nets. *Advances in neural information processing systems* 27 (2014).

[11] Amir Hertz, Ron Mokady, Jay Tenenbaum, Kfir Aberman, Yael Pritch, and Daniel Cohen-Or. 2022. Prompt-to-prompt image editing with cross attention control. *arXiv preprint arXiv:2208.01626* (2022).

[12] Jonathan Ho, Ajay Jain, and Pieter Abbeel. 2020. Denoising diffusion probabilistic models. *Advances in neural information processing systems* 33 (2020), 6840–6851.

[13] Edward J Hu, Yelong Shen, Phillip Wallis, Zeyuan Allen-Zhu, Yuanzhi Li, Shean Wang, Lu Wang, and Weizhu Chen. 2021. Lora: Low-rank adaptation of large language models. *arXiv preprint arXiv:2106.09685* (2021).

[14] Bahjat Kawar, Shiran Zada, Oran Lang, Omer Tov, Huiwen Chang, Tali Dekel, Inbar Mosseri, and Michal Irani. 2023. Imagic: Text-based real image editing with diffusion models. In *Proceedings of the IEEE/CVF Conference on Computer Vision and Pattern Recognition*. 6007–6017.

[15] Gwanghyun Kim, Taesung Kwon, and Jong Chul Ye. 2022. Diffusionclip: Text-guided diffusion models for robust image manipulation. In *Proceedings of the IEEE/CVF Conference on Computer Vision and Pattern Recognition*. 2426–2435.

[16] Junnan Li, Dongxu Li, Caiming Xiong, and Steven Hoi. 2022. Blip: Bootstrapping language-image pre-training for unified vision-language understanding and generation. In *International conference on machine learning*. PMLR, 12888–12900.

[17] Yuheng Li, Haotian Liu, Qingyang Wu, Fangzhou Mu, Jianwei Yang, Jianfeng Gao, Chunyuan Li, and Yong Jae Lee. 2023. GLIGEN: Open-Set Grounded Text-to-Image Generation. In *Proc. IEEE Conf. CVPR*. IEEE, 22511–22521. <https://doi.org/10.1109/CVPR52729.2023.02156>

[18] Simian Luo, Yiqin Tan, Longbo Huang, Jian Li, and Hang Zhao. 2023. Latent consistency models: Synthesizing high-resolution images with few-step inference. *arXiv preprint arXiv:2310.04378* (2023).

[19] Simian Luo, Yiqin Tan, Suraj Patil, Daniel Gu, Patrick von Platen, Apolinário Passos, Longbo Huang, Jian Li, and Hang Zhao. 2023. Lcm-lora: A universal stable-diffusion acceleration module. *arXiv preprint arXiv:2311.05556* (2023).

[20] Hayk Manukyan, Andranik Sargsyan, Barsegh Atanyan, Zhangyang Wang, Shant Navasardyan, and Humphrey Shi. 2023. HD-Painter: High-Resolution and Prompt-Faithful Text-Guided Image Inpainting with Diffusion Models. *arXiv preprint arXiv:2312.14091* (2023).

[21] Ron Mokady, Amir Hertz, Kfir Aberman, Yael Pritch, and Daniel Cohen-Or. 2023. Null-text inversion for editing real images using guided diffusion models. In *Proceedings of the IEEE/CVF Conference on Computer Vision and Pattern Recognition*. 6038–6047.

[22] Chong Mou, Xintao Wang, Liangbin Xie, Yanze Wu, Jian Zhang, Zhongang Qi, and Ying Shan. 2024. T2i-adapter: Learning adapters to dig out more controllable ability for text-to-image diffusion models. In *Proceedings of the AAAI Conference on Artificial Intelligence*, Vol. 38. 4296–4304.

[23] Alex Nichol, Prafulla Dhariwal, Aditya Ramesh, Pranav Shyam, Pamela Mishkin, Bob McGrew, Ilya Sutskever, and Mark Chen. 2021. Glide: Towards photorealistic image generation and editing with text-guided diffusion models. *arXiv preprint arXiv:2112.10741* (2021).

[24] William Peebles and Saining Xie. 2023. Scalable diffusion models with transformers. In *Proceedings of the IEEE/CVF International Conference on Computer Vision*. 4195–4205.

[25] Dustin Podell, Zion English, Kyle Lacey, Andreas Blattmann, Tim Dockhorn, Jonas Müller, Joe Penna, and Robin Rombach. 2023. Sdxl: Improving latent diffusion models for high-resolution image synthesis. *arXiv preprint arXiv:2307.01952* (2023).

[26] Alec Radford, Jong Wook Kim, Chris Hallacy, Aditya Ramesh, Gabriel Goh, Sandhini Agarwal, Girish Sastry, Amanda Askell, Pamela Mishkin, Jack Clark, et al. 2021. Learning transferable visual models from natural language supervision. In *International conference on machine learning*. PMLR, 8748–8763.

[27] Colin Raffel, Noam Shazeer, Adam Roberts, Katherine Lee, Sharan Narang, Michael Matena, Yanqi Zhou, Wei Li, and Peter J Liu. 2020. Exploring the limits of transfer learning with a unified text-to-text transformer. *Journal of machine learning research* 21, 140 (2020), 1–67.

[28] Colin Raffel, Noam Shazeer, Adam Roberts, Katherine Lee, Sharan Narang, Michael Matena, Yanqi Zhou, Wei Li, and Peter J. Liu. 2020. Exploring the Limits of Transfer Learning with a Unified Text-to-Text Transformer. *Journal of Machine Learning Research* 21, 140 (2020), 1–67. <http://jmlr.org/papers/v21/20-074.html>

[29] Aditya Ramesh, Prafulla Dhariwal, Alex Nichol, Casey Chu, and Mark Chen. 2022. Hierarchical text-conditional image generation with clip latents. *arXiv preprint arXiv:2204.06125* 1, 2 (2022), 3.

[30] Robin Rombach, Andreas Blattmann, Dominik Lorenz, Patrick Esser, and Björn Ommer. 2022. High-resolution image synthesis with latent diffusion models. In *Proceedings of the IEEE/CVF conference on computer vision and pattern recognition*. 10684–10695.

[31] Nataniel Ruiz, Yuanzhen Li, Varun Jampani, Yael Pritch, Michael Rubinstein, and Kfir Aberman. 2023. Dreambooth: Fine tuning text-to-image diffusion models for subject-driven generation. In *Proceedings of the IEEE/CVF Conference on Computer Vision and Pattern Recognition*. 22500–22510.

[32] Chitwan Saharia, William Chan, Saurabh Saxena, Lala Li, Jay Whang, Emily L Denton, Kamyar Ghasemipour, Raphael Gontijo Lopes, Burcu Karagol Ayan, Tim Salimans, et al. 2022. Photorealistic text-to-image diffusion models with deep language understanding. *Advances in neural information processing systems* 35

- (2022), 36479–36494.
- [33] Tim Salimans and Jonathan Ho. 2022. Progressive distillation for fast sampling of diffusion models. *arXiv preprint arXiv:2202.00512* (2022).
 - [34] Axel Sauer, Dominik Lorenz, Andreas Blattmann, and Robin Rombach. 2023. Adversarial diffusion distillation. *arXiv preprint arXiv:2311.17042* (2023).
 - [35] James Seale Smith, Yen-Chang Hsu, Lingyu Zhang, Ting Hua, Zsolt Kira, Yilin Shen, and Hongxia Jin. 2023. Continual diffusion: Continual customization of text-to-image diffusion with c-lora. *arXiv preprint arXiv:2304.06027* (2023).
 - [36] Jiaming Song, Chenlin Meng, and Stefano Ermon. 2020. Denoising diffusion implicit models. *arXiv preprint arXiv:2010.02502* (2020).
 - [37] Yang Song, Prafulla Dhariwal, Mark Chen, and Ilya Sutskever. 2023. Consistency models. *arXiv preprint arXiv:2303.01469* (2023).
 - [38] Yang Song and Stefano Ermon. 2019. Generative modeling by estimating gradients of the data distribution. *Advances in neural information processing systems* 32 (2019).
 - [39] Ming Tao, Hao Tang, Fei Wu, Xiao-Yuan Jing, Bing-Kun Bao, and Changsheng Xu. 2022. Df-gan: A simple and effective baseline for text-to-image synthesis. In *Proceedings of the IEEE/CVF Conference on Computer Vision and Pattern Recognition*. 16515–16525.
 - [40] Narek Tumanyan, Michal Geyer, Shai Bagon, and Tali Dekel. 2023. Plug-and-play diffusion features for text-driven image-to-image translation. In *Proceedings of the IEEE/CVF Conference on Computer Vision and Pattern Recognition*. 1921–1930.
 - [41] Tao Xu, Pengchuan Zhang, Qiuyuan Huang, Han Zhang, Zhe Gan, Xiaolei Huang, and Xiaodong He. 2018. AttnGAN: Fine-grained text to image generation with attentional generative adversarial networks. In *Proceedings of the IEEE conference on computer vision and pattern recognition*. 1316–1324.
 - [42] Ahmet Burak Yildirim, Vedat Baday, Erkut Erdem, Aykut Erdem, and Aysegul Dundar. 2023. Inst-inpaint: Instructing to remove objects with diffusion models. *arXiv preprint arXiv:2304.03246* (2023).
 - [43] Tao Yu, Runseng Feng, Ruoyu Feng, Jinming Liu, Xin Jin, Wenjun Zeng, and Zhibo Chen. 2023. Inpaint anything: Segment anything meets image inpainting. *arXiv preprint arXiv:2304.06790* (2023).
 - [44] Han Zhang, Jing Yu Koh, Jason Baldridge, Honglak Lee, and Yinfei Yang. 2021. Cross-modal contrastive learning for text-to-image generation. In *Proceedings of the IEEE/CVF conference on computer vision and pattern recognition*. 833–842.
 - [45] Lvmin Zhang, Anyi Rao, and Maneesh Agrawala. 2023. Adding conditional control to text-to-image diffusion models. In *Proceedings of the IEEE/CVF International Conference on Computer Vision*. 3836–3847.
 - [46] Minfeng Zhu, Pingbo Pan, Wei Chen, and Yi Yang. 2019. Dm-gan: Dynamic memory generative adversarial networks for text-to-image synthesis. In *Proceedings of the IEEE/CVF conference on computer vision and pattern recognition*. 5802–5810.

A MORE EXAMPLES

We first provide more small objects generated by our SOEDiff in Fig. 9. Then we show more ablation results in Fig. 10 to prove the effectiveness of our main components **SO-LoRA** and **Cross-Scaled Distillation**. Additionally, more extended applications results, mainly including object erasing and object replacement, are shown in Fig. 11.

Our project page can be found <https://soediff.github.io/>.

B MORE COMPARISON RESULTS

Compare with more methods [2, 20, 30, 43] and the results are shown in Tab. 6. The Inpaint-Anything using Stable-Diffusion-2-Inpainting as default. And comparison results are shown in Fig. 12. In addition to comparisons with different models, we also evaluated another method for generating small objects, similar to the approach mentioned in the article where the teacher processes images by cropping the original image. The new image obtained has a mask area with sides at least twice the length of the original, transforming the small object generation issue into a somewhat simpler problem. This is referred to as the "cropped-method" in the table. It can be observed that our method also achieves better result. Mainly because this approach has inherent disadvantages, such as the loss

of the overall image context information. This can sometimes lead to less effective results.

Table 6: Quantitative results on *OpenImage-f* and *MSCOCO-f*. SOEDiff significantly surpasses the baselines. The best results are highlighted in bold.

Prompt	Methods	OpenImage-f		MSCOCO-f	
		CLIP-Score	FID	CLIP-Score	FID
label	Blended DM	23.66	43.20	22.83	38.78
	SD-I	23.79	34.65	22.55	30.78
	Inpaint-Anything	24.09	33.52	22.81	29.38
	HD-Painter	24.39	32.74	23.25	29.97
	SOEDiff	24.78	31.78	23.89	29.40
color + label	cropped-method	24.51	32.84	23.42	30.21
	Blended DM	23.85	43.26	22.94	38.01
	SD-I	24.13	34.73	22.66	30.65
	Inpaint-Anything	24.50	33.69	23.02	28.92
	HD-Painter	25.19	32.35	23.98	29.01
SOEDiff	25.57	31.21	24.38	27.62	
cropped-method	25.11	32.45	24.03	28.49	

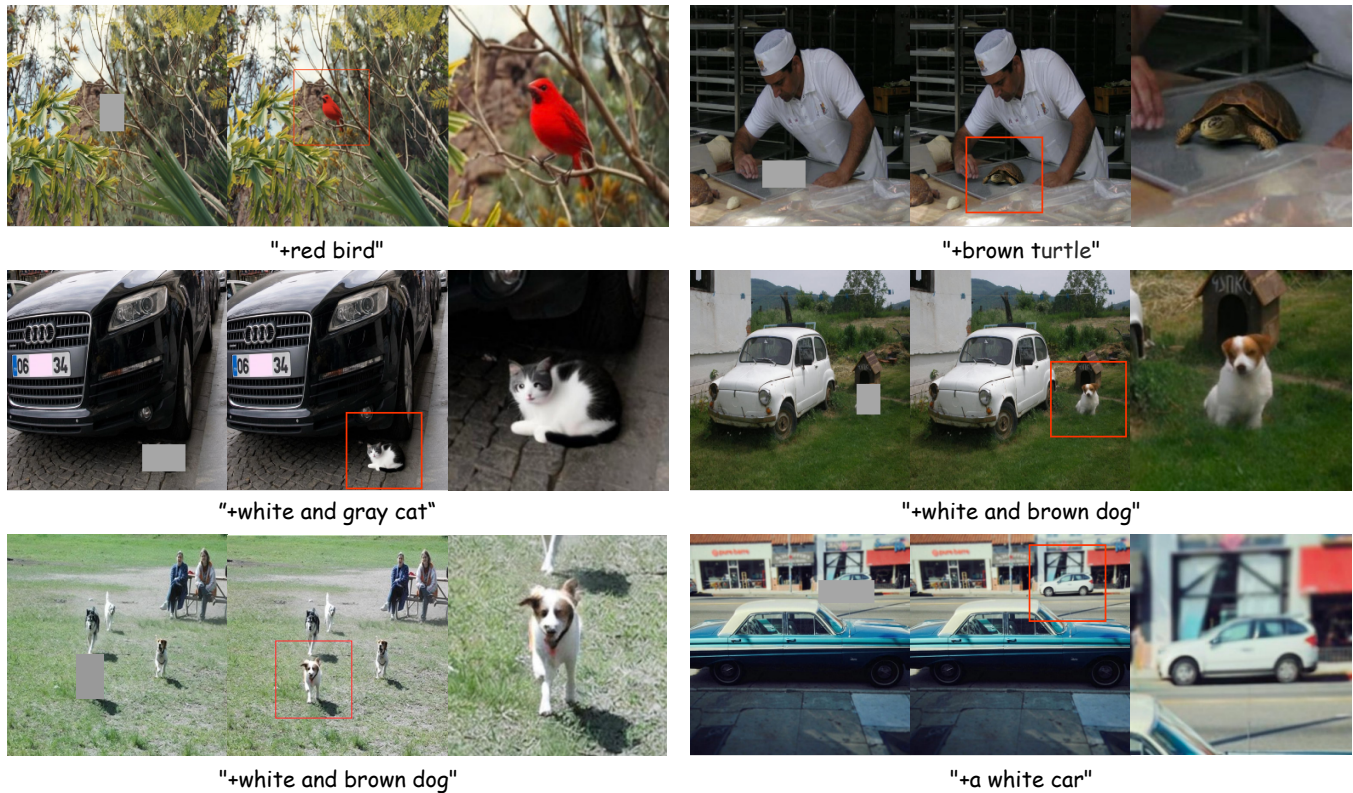


Figure 9: More small objects generated by our SOEDiff. The first column displays the input images and corresponding masks, the second column shows the generated images, and the third column features close-up views to highlight more detailed parts of the objects.



Figure 10: More examples to show the effectiveness of our components. The first row displays the results generated by SD-I, the second row shows the generated images with SD-I+SO-LoRA, and the third row shows the results generated by SOEDiff.

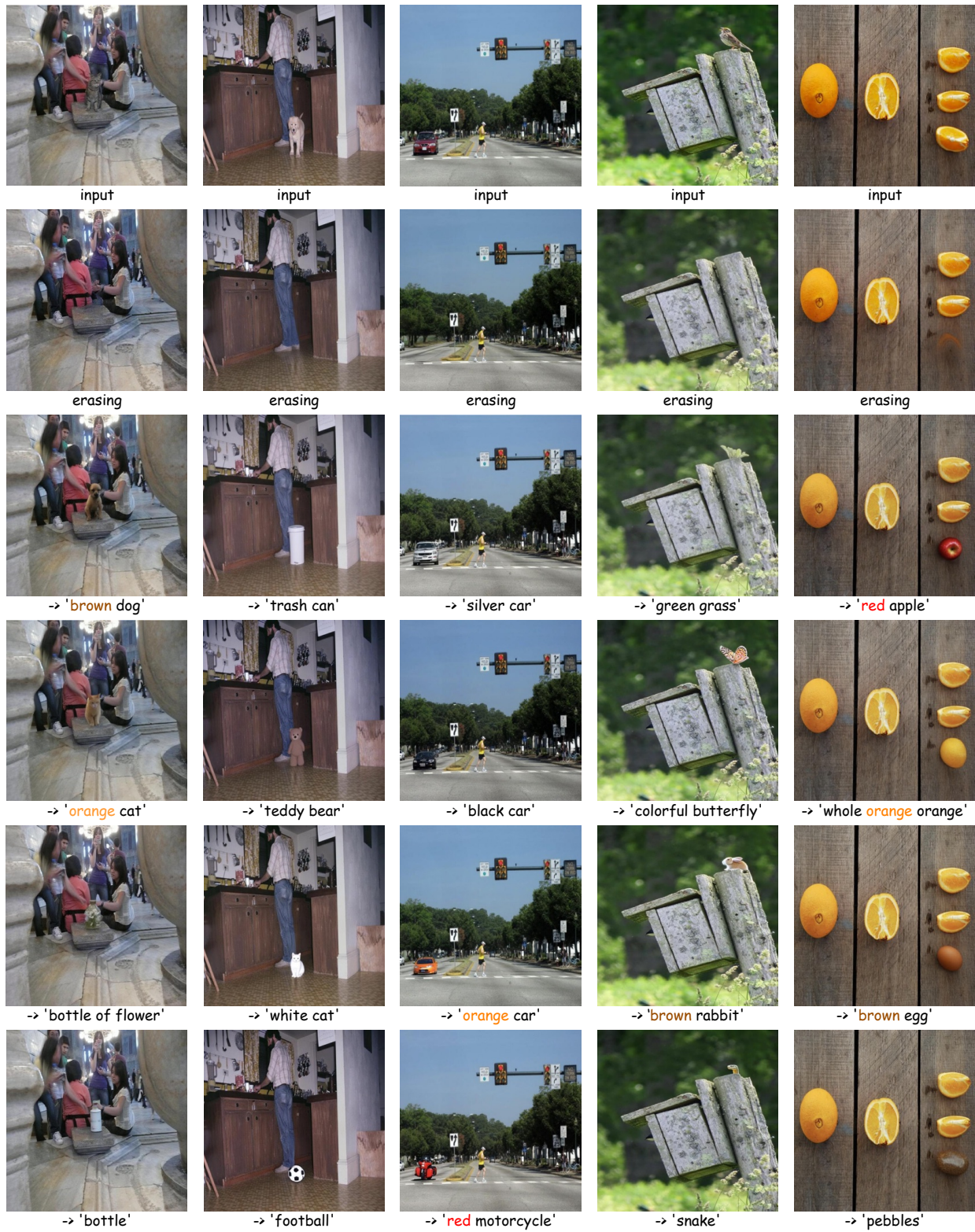


Figure 11: Extended application with our proposed SOEDiff. The first row shows the original images, the second row displays the results of object erasing, and rows three to six depict the results of object replacement.

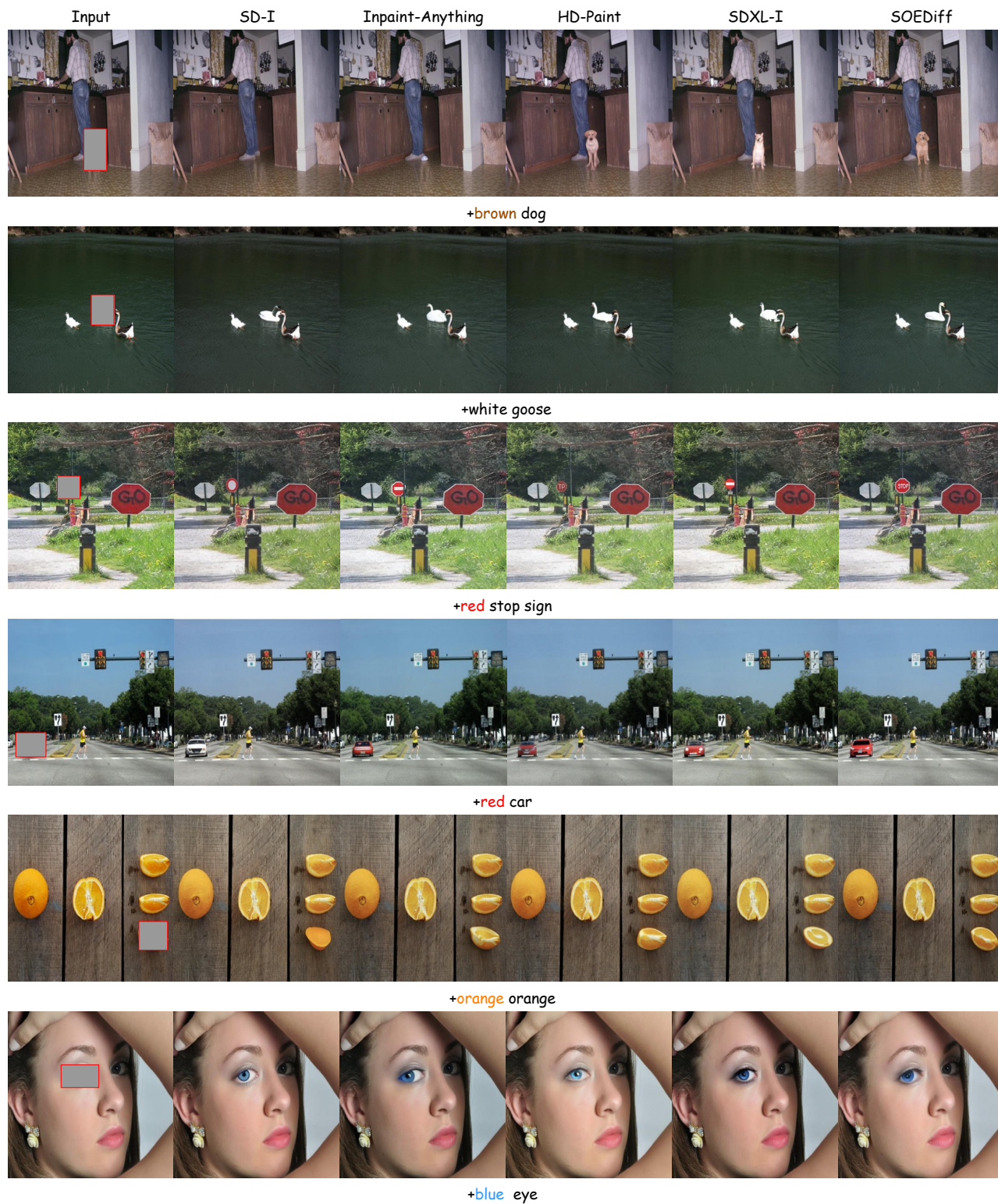


Figure 12: Comparing results between our methods and other models. The first column represents the input original images and corresponding masks, while the second to sixth columns show the results generated by SD-I, Inpaint-Anything, HD-painter, SDXL-I, and SOEDiff, respectively.